Size determination of microbubbles in optical microscopy: a best-case scenario

Michiel Postema, Habtamu Abraham, Ondrej Krejcar, Dawit Assefa

Research Article | Vol. 25, No. 26 | 25 Dec 2017 | OPTICS EXPRESS 33588
Optics EXPRESS

Size determination of microbubbles in optical microscopy: a best-case scenario

MICHIEL POSTEMA,[1,2,3] HABTAMU ABRAHAM,[4] ONDREJ KREJCAR,[5] AND DAWIT ASSEFA[5,6,*]

[1]*LE STUDIUM Loire Valley Institute for Advanced Studies, 1 Rue Dupanloup 45000, Orléans, France*
[2]*INSERM Research Unit U930: Imaging and Brain, UFR Médecine, 10 Boulevard Tonnellé 37032, Tours, France*
[3]*School of Electrical and Information Engineering, Chamber of Mines Building, University of the Witwatersrand, 1 Jan Smuts Avenue, Braamfontein, Johannesburg 2050, South Africa*
[4]*School of Electrical and Computer Engineering, Biomedical Engineering Department, Hawassa Institute of Technology, Hawassa University, Hawassa, Ethiopia*
[5]*Center for Basic and Applied Research, Faculty of Informatics and Management University of Hradec Kralove, Hradec Kralove, Czech Republic*
[6]*Center of Biomedical Engineering, Division of Biomedical Computing, Addis Ababa Institute of Technology, Addis Ababa University, Addis Ababa, Ethiopia*
[*]*dawit.assefa@aau.edu.et*

Abstract: Microbubble-based ultrasound contrast agents are used in clinical settings to enhance backscattered ultrasound signals from blood during perfusion and blood flow measurements. The dynamics of microbubbles contained in ultrasound contrast agents are typically studied with a high-speed camera attached to a microscope. Such microbubbles, with resting diameters between 1 μm and 7 μm, are considered in optical focus if the bubble centers are in the focal plane of the objective lens. Nonetheless, when a three-dimensional object, a stack of infinitely thin two-dimensional layers, is imaged through a microscope, the image formed onto the charge coupled device element consists of contributions from all layers. If a bubble is larger than the depth of focus, the part of the bubble above the focal plane influences the image formation and therefore the bubble size measured. If a bubble is of a size in the order of the wavelengths of the light used, the system resolution and the segmentation method influence the bubble size measured. In this study, the projections of three dimensional microbubbles (hollow spheres) were computed with an ideal, weighted three-dimensional point spread function to find out under which circumstances the optical image formation leads to a significant deviation in measurement of the actual size. The artificial images were subjected to segmentation techniques for objectively comparing original microbubble sizes with measured microbubble sizes. Results showed that a systematic error was observed for objects in focus with radius $\leq 1.65\mu$m. Also it was concluded that even though a three-dimensional object is in focus, there is discrepancy of up to 0.66% in size measurement. In addition, size measurement of an object for the same shift above and below focus could differ by up to 3.6%. Moreover, defocusing above 25% severely deviates size measurements while defocusing up to 90% could result in mean percentage error of up to 67.96.

OCIS codes: (110.0110) Imaging systems; (110.1758) Computational imaging.

References and links

1. A. L. Klibanov, P. T. Rasche, M. S. Hughes, J. K. Wojdyla, K. P. Galen, J. H. Wible Jr, and G. H. Brandenburger, "Detection of individual microbubbles of ultrasound contrast agents: imaging of free-floating and targeted bubbles," Invest. Radiol. **39** (3), 187–195 (2004).
2. C. -D. Ohl, T. Kurz, R. Geisler, O. Lindau, and W. Lauterborn, "Bubble dynamics, shock waves and sonoluminescence," Philos. Trans. Roy. Soc. A **357** 269–294 (1999).
3. M. Postema, A. Bouakaz, C. T. Chin, and N. de Jong, "Simulations and measurements of optical images of insonified ultrasound contrast microbubbles," IEEE Trans. Ultrason. Ferroelectr. Freq. Control **50** (5), 523–536 (2003).

#307837 https://doi.org/10.1364/OE.25.033588
Journal © 2017 Received 18 Oct 2017; revised 11 Dec 2017; accepted 16 Dec 2017; published 22 Dec 2017

Optics EXPRESS

4. K. Okada, N. Kudo, K. Niwa, and K. Yamamoto, "A basic study on sonoporation with microbubbles exposed to pulsed ultrasound," J. Med. Ultrason. **32** (1), 3–11 (2005).
5. P. Prentice, A. Cuschieri, K. Dholakia, M. Prausnitz, and P. Campbell, "Membrane disruption by optically controlled microbubble cavitation," Nature Phys. **1** (2), 107–110 (2005).
6. H. Netten, L. J. van Vliet, F. R. Boddeke, P. de Jong, and I. T. Young, "A fast scanner for fluorescence microscopy using a 2-D CCD and time delayed integration," Bioimaging **2** (4), 184–192 (1994).
7. J. -B. Sibarita, "Deconvolution microscopy," Adv. Biochem. Eng./Biotechnol. **95**, 201–243 (2005).
8. D. A. Agard, "Optical sectioning microscopy: Cellular architecture in three dimensions," Annu. Rev. Biophys. Bioeng. **13**, 191–219 (1984).
9. I. T. Young, "Quantitative microscopy," IEEE Eng. Med. Biol. **15** (1), 59–66 (1996).
10. M. Postema, *Fundamentals of Medical Ultrasonics* (CRC Press, 2011).
11. Q. Wu, F. A. Merchant, K. R. Castleman, *Microscope Image Processing* (Elsevier, 2008).
12. S. Kotopoulis, M. Postema, "Microfoam formation in a capillary," Ultrasonics **50**, 260–268 (2010).
13. B. Matérn, "Precision of area estimation: a numerical study," J. Microsc. **153**, 269–284 (1989).

1. Introduction

Observing the dynamics of acoustically active microbubbles has been of major interest in medical imaging and therapy, but also in the hydrocarbon industry. The microbubbles in so-called ultrasound contrast agents consist of perfluorocarbon gas bubbles surrounded by an encapsulating lipid or albumin shell. These microbubbles are typically between 1 μm and 7 μm in diameter. The most common means of observing bubbles in a sound field is high-speed photography through a microscope setup during sonication [1–5].

A three-dimensional object under a microscope can be considered as a stack of thin two-dimensional layers [6]. When three-dimensional objects are observed through a microscope, the projection consists of contributions from all of these layers. A bubble is considered in focus if the middle layer of the sphere is in the focal plane. If a bubble is larger than the depth of focus, the part of the bubble above the focal plane influences the projection and therefore the bubble size measured. Consequently, images from an axial shift above the focal plane are not identical to the images from the same shift below the focal plane. If a bubble is of a size in the order of the wavelengths of the light used, the system resolution and the segmentation method influence the bubble size measured.

In a previous study, comparing real images to simulations of a two-dimensional point spread function on circular objects, no systematic error was found when measuring the size of microbubbles with diameters of 0.8 μm and greater [3]. However, the influence of the contribution of the bubble parts above and below the focal plane were discarded.

The objective of the current study was to find whether a systematic error occurs when measuring microbubbles in focus, when taking into account all layers contributing to the image. With this aim, the projections of microbubbles (assumed hollow spheres) were computed with an ideal three-dimensional point spread function to find out under which circumstances the optical image formation leads to a significant deviation in measurement of the actual size. The artificial images were subjected to segmentation techniques for objectively comparing original microbubble sizes with measured microbubble sizes.

2. Theory

Let us consider a noise-free situation. Then, the image from an ideal microscope can be expressed in xyz-coordinates by [7]:

$$i(x, y, z) = \int\int\int o(x', y', z')h(x - x', y - y', z - z')dx'dy'dz', \tag{1}$$

where i is the image, o is the object imaged, and h is the point spread function of the optical imaging system. Knowing that a three-dimensional object under a microscope can be considered

Optics EXPRESS

as a stack of thin two-dimensional layers, the image of an object in the focal plane can be computed with the weighed sum of each contributing layer:

$$i(x, y) = \sum_z \Big(w(z) \int \int o(x', y', z) h(x - x', y - y') dx' dy' \Big), \tag{2}$$

where w is a weighing function.

Furthermore, as the microscope is ideal, we may assume a circularly symmetric point spread function in the focal plane [3, 8, 9]:

$$h(r) = \Big[\frac{2J_1(ar)}{ar} \Big]^2, \tag{3}$$

where J_1 is the first-order Bessel function of the first kind, $r = \sqrt{x^2 + y^2}$, and

$$a = \frac{2\pi n sin(\theta)}{\lambda} = \frac{2\pi NA}{\lambda}, \tag{4}$$

in which n is the refractive index of the medium between the lens and the object, θ is the angle of acceptance of the objective lens, λ is the wavelength of the light, and NA is the numerical aperture of the objective lens.

Figure 1 illustrates 1D, 2D and 3D ideal PSFs generated using parameters $\lambda = 500$nm, $NA = 1.25$ and $n = 1.3$. The distance Δz over which an object can be observed without significant

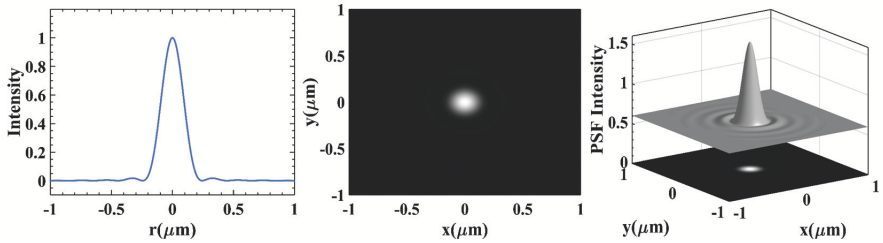

Fig. 1. Simulation of ideal PSF in: 1D (left), 2D (middle) and 3D using parameters $\lambda = 500$nm, $NA = 1.25$ and $n = 1.3$.

optical aberration is called the depth of focus. It is given by [9]:

$$\Delta z = \frac{\lambda}{4n\Big[1 - \sqrt{1 - \big(\frac{NA}{n}\big)^2}\Big]}, \tag{5}$$

As a consequence, when computing (2), choosing layers with a thickness less than Δz would have no influence on the resulting image.

The weighing function w has a form similar to the intensity field from a circular piston [10]:

$$w(z) \propto \Big| sin\Big(\frac{\pi R^2}{2\lambda z}\Big) \Big|, \tag{6}$$

where R is the radius of the objective lens.

Once an optical image of a microbubble is recorded, the process of size measurement can be done in an automated fashion. The most common method to discriminate dark objects from a light background is to segment the image using grey-level window-slicing [11]:

$$\xi(x, y) = \begin{cases} 1, & o(x, y) \le T, \\ 0, & o(x, y) > T. \end{cases} \tag{7}$$

where ξ is the segmented image and T is the threshold grey-level.

Optics EXPRESS

3. Methods

To generate artificial optical images, the two-dimensional point spread function in (3) was computed, using $NA = 1.25$ and $\lambda = 500$nm in (4). Sixteen layers, each of thickness $\Delta z = 133$nm, were used to compute the weighing functions from (6), in which $R = 1.75$mm and $1.75\text{mm} \leq z \leq 1.76\text{mm}$. Please note, that the parameters chosen to describe the optical system were unrealistically superb compared to those of the actual experimental setup in, e.g., [3, 12].
The object functions were spheres with radius r, represented by white circles on a black background or black circles on a white background in each of the 16 layers. Ring thickness (R_t) is taken to be 200nm, assuming a polymer encapsulating layer. The white ring objects with black background were created using the following function in 3D:

$$o(x, y, z) = \begin{cases} 1, & (x^2 + y^2 + z^2) \leq r^2, \ \ (x^2 + y^2 + z^2) \geq (r - R_t)^2 \\ 0, & \text{Otherwise} \end{cases} \tag{8}$$

Similarly the black ring with white background artificial images could be generated easily.

After convolution with the respective weighed point spread function, the resulting two-dimensional images were stacked and normalised, according to (2). Resampling was done to have each image pixel correspond to a $0.15 \times 0.15\ (\mu m)^2$ area. The radius range of the object spheres varied from $0.5\mu m$ to $5.0\mu m$. Simulated 3D sphere objects with different radii are illustrated in Fig. 2. Image segmentation was done with a threshold $T = 0.5$, knowing that the artificial images

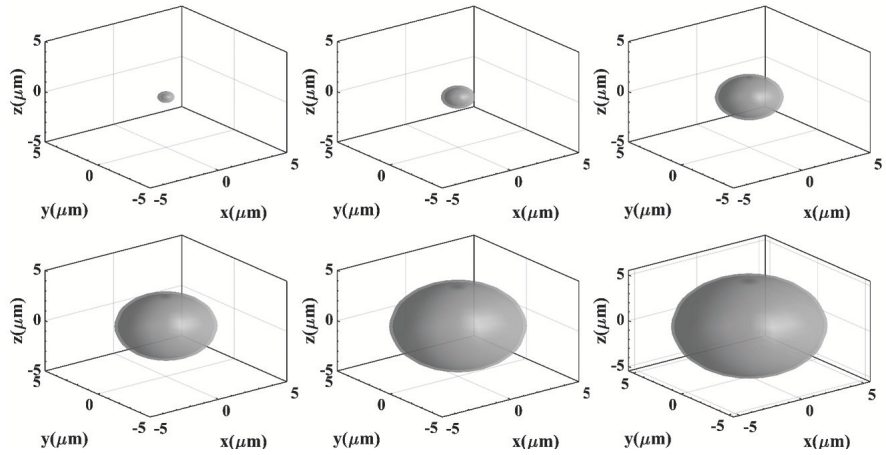

Fig. 2. Simulation of 3D objects with radius 0.5μm, 1μm, 2μm, 3μm, 4μm, and 5μm: from top left to bottom right.

represent perfect black-and-white images [3]. The bubble area A was measured by summation of all points in the segmented area [9, 13], yielding the measured bubble radius $R = \sqrt{\frac{A}{\pi}}$.

4. Results and discussion

Weighting functions generated above and near the focus are shown in Fig. 3 while Fig. 4 illustrates an ideal 1D PSF, 1D weighing function (assuming 16 layers) and the resulting 1D weighted PSFs as well as 2D weighted PSFs.

4.1. Slicing white ring and black ring objects

As mentioned earlier, a 3D object can be considered as a stack of infinitely thin two-dimensional layers and when 3D objects are imaged through a microscope, the image formed onto the charge

Optics EXPRESS

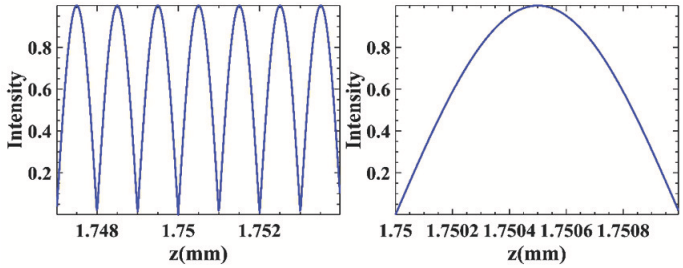

Fig. 3. Weighting function profile: Above the focus (1.747mm $\leq z \leq$ 1.756mm) (left) and near the focus (right) for Δz = 133nm.

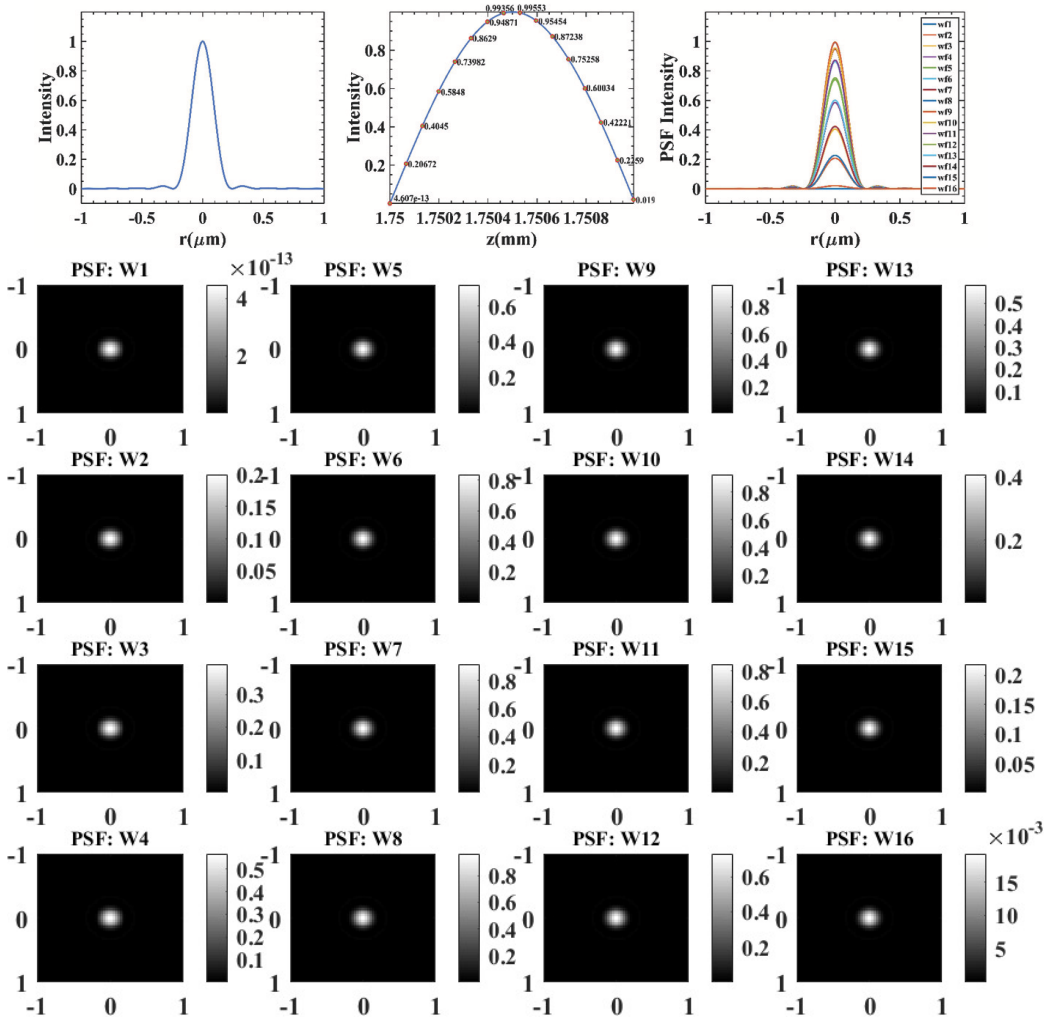

Fig. 4. Simulation of Ideal 1D PSF (top left), 1D weighing function with 16 layers (top middle), 1D weighted PSFs (top right), and 16 2D weighted PSFs corresponding to the 16 layers.

Optics EXPRESS

coupled device (CCD) element consists of contributions from all layers. Hence, to take into account the contribution of each layer in 3D objects, each object is sliced based on the optical system depth of focus. The depth of focus was computed using (5) for $n = 1.3$, and $\lambda = 500$ nm and typical sliced objects look like the ones depicted in Fig. 5.

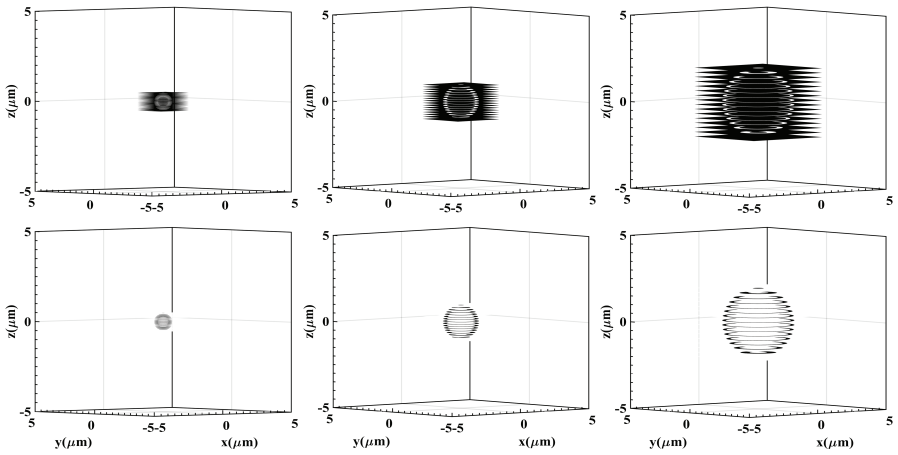

Fig. 5. Slices of white ring objects (first row) and black ring objects (second row) with radius and slice depth of: $0.5\mu m$ and $0.5 * \Delta z$; $1\mu m$ and $1 * \Delta z$; and $2\mu m$ and $2 * \Delta z$ respectively from left to right. Note that multiples of Δz were used for each object to visualize same (16) number of slices with out overlapping. However, for the actual size measurement $\Delta z = 133nm$.

4.2. Simulating shift of focus

Microbubbles are often observed through microscope under the influence of an ultrasound and it is likely that they get out of focus. As a result, when seen under an image capturing device, their images would be blurred and their size measures would deviate from the actual size measurement. Therefore, measuring the microbubbles size while they are out of focus would help to analyze the effect of defocussing while quantifying bubbles dimension. Consequently, it is possible to predict the actual size of bubbles even though they are imaged out of focus. The simulation of shift of focus for both small objects and large objects is shown in Fig. 6 (shown for white rings with dark background) and Fig. 7 (shown for dark rings with white background) respectively. It can be seen on the figures that small objects interfere with small portion of the light while large objects behave the opposite. When an object is in focus, all slices contribute during image formation. Hence, they are weighted with their full size in focus (green region). On the other hand, when an object is out of focus, it is weighted only by the portion of the light where the object is in focus.

4.3. 2D Image formation

An optical image of a radially symmetric flat object in focus, observed through a microscope, is expressed by convolution of the PSF of the optical system and the object. Hence, to compute the 2D image formed at the CCD, first the 3D object slices (shown for the white rings in Fig. 8) are convolved with the weighted PSFs. The convolution result (shown in Fig. 9 for the white rings in Fig. 8) shows that near the focus the intensity is higher as seen on the intensity bar. Similar results could be generated for the black rings. What is typically different is the blurring effect of the PSF. The blurring effect of the PSF when convolved with the white rings and the black rings is illustrated in Fig. 10 and Fig. 11 respectively. In order to then form a 2D image, the convolved object slices are stacked and summed. The segmented 2D images for the white ring and black

Optics EXPRESS

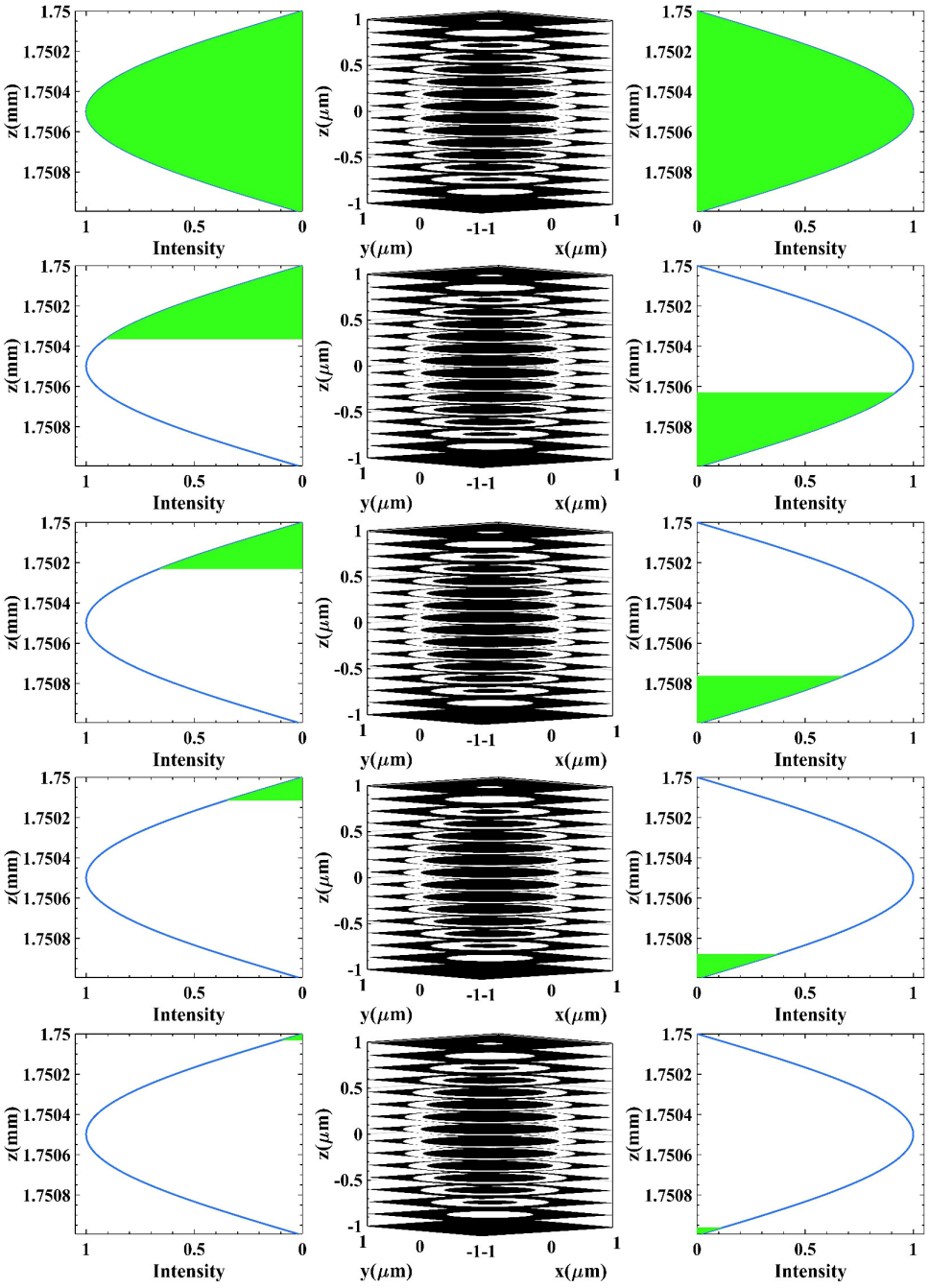

Fig. 6. Simulation of shift of focus (green region) for objects of radius $r = 0.5\mu m$. First column is above focus, third column is below focus while the middle column is the 3D object. Going from the second row to the last, the shift is 25%, 50%, 75%, and 90% respectively.

Optics EXPRESS

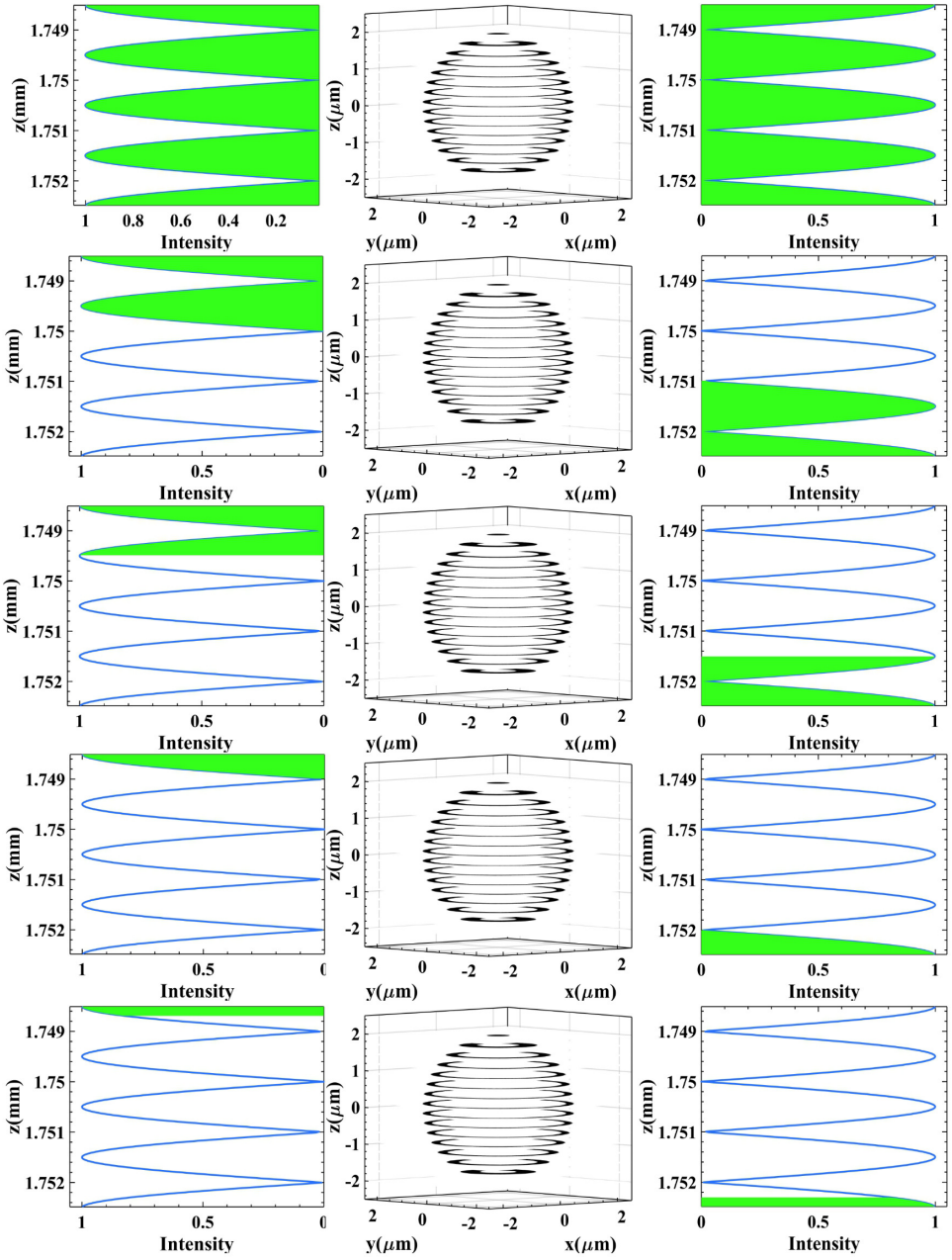

Fig. 7. Simulation of shift of focus (green region) for objects of radius $r = 2\mu m$. First column is above focus, third column is below focus while the middle column is the 3D object. Going from the second row to the last, the shift is 25%, 50%, 75%, and 90% respectively.

Optics EXPRESS

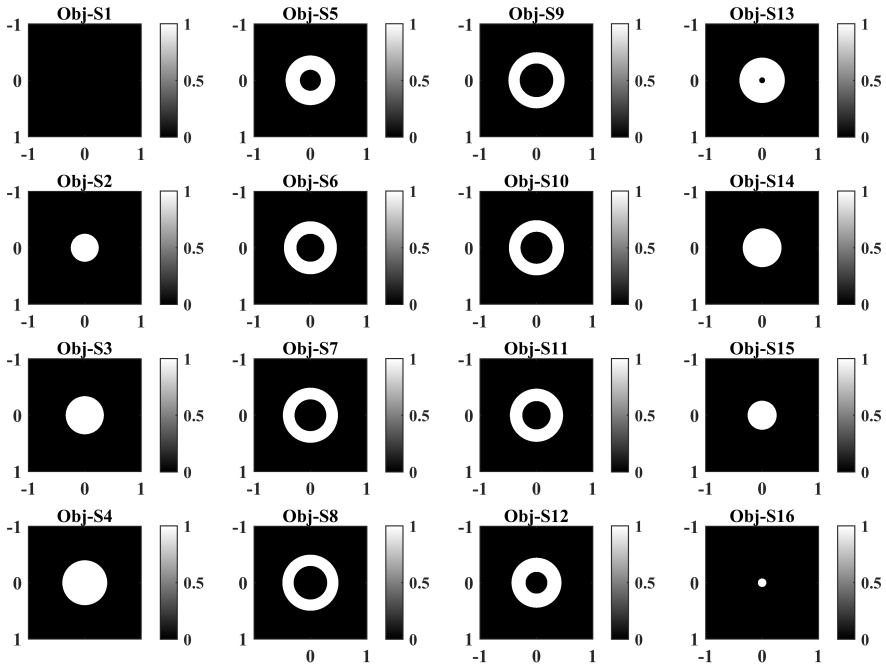

Fig. 8. 16 2D slice images of 3D object taken with $0.5 * \Delta z$ for radius of $r = 0.5\mu m$.

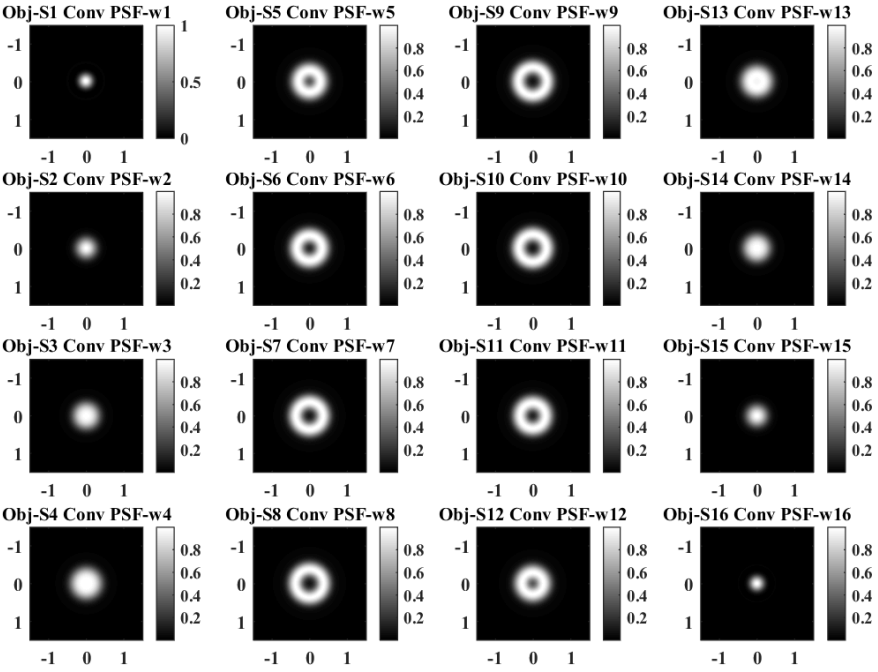

Fig. 9. Simulation of convolution between 16 weighted PSFs and object slices. Convolution result is normalized.

Optics EXPRESS

ring objects (which were presented in Fig. 10 and Fig. 11) are shown in Fig. 12 and Fig. 13 respectively.

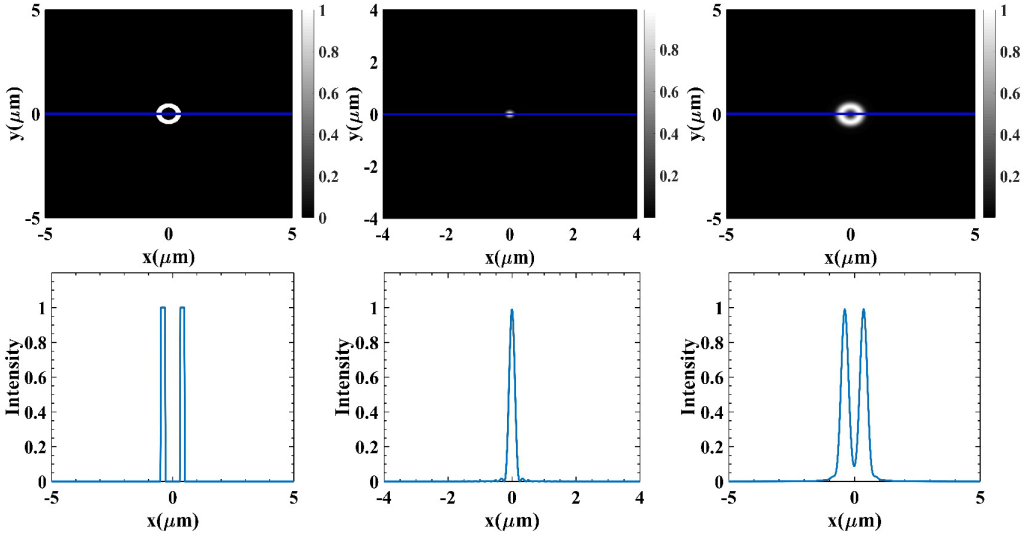

Fig. 10. Effects of PSF on slices during convolution: White ring object slice at the focus (left), 2D PSF at the focus (middle), and Convolved slice (right). Second row shows intensity cross-sections of the respective images in the first row.

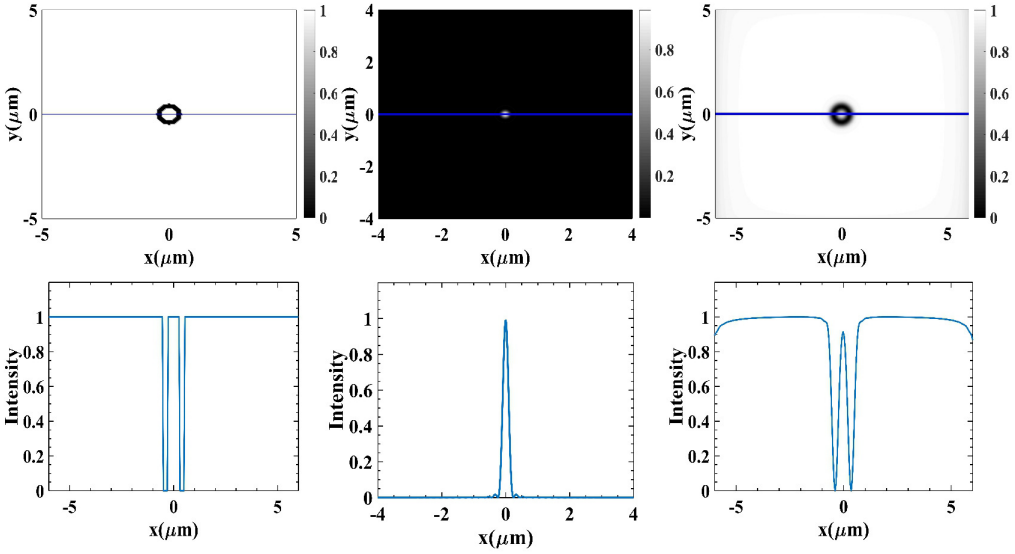

Fig. 11. Effects of PSF on slices during convolution: Black ring object slice at the focus (left), 2D PSF at the focus (middle), and Convolved slice (right). Second row shows intensity cross-sections of the respective images in the first row

Optics EXPRESS

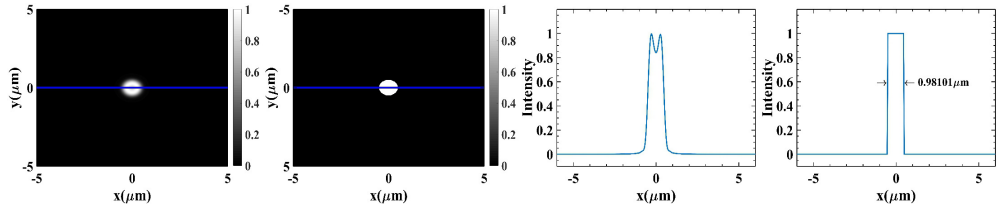

Fig. 12. Segmentation of 16 stacked white ring object slices: the first two images are stacked weighed object slices and segmented object while the last two are the respective intensity cross-sections respectively.

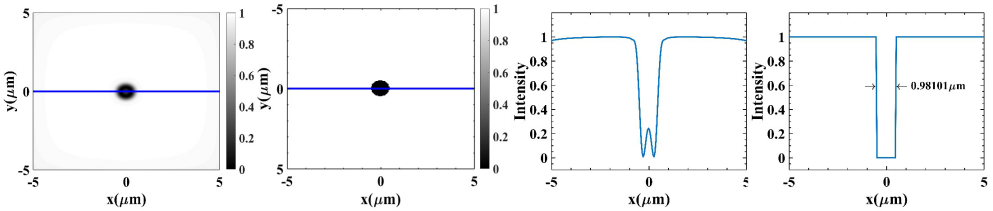

Fig. 13. Segmentation of 16 stacked black ring object slices: the first two images are stacked weighed object slices and segmented object while the last two are the respective intensity cross-sections respectively.

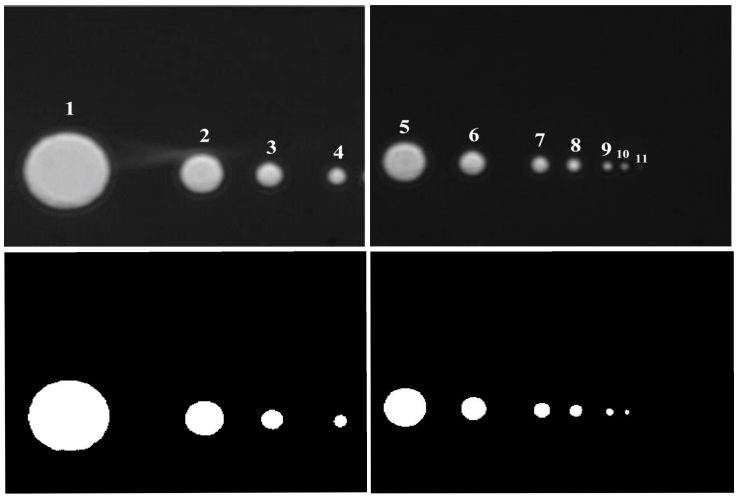

Fig. 14. CCD images of 11 triacontakaidigons on a calibration grid (first row) segmented with a $\theta = 1/2(u' + v')$ threshold, where u' is median intensity and v' is median background value (bottom row) [3].

Optics EXPRESS

4.4. True versus measured 2D object size

Before quantifying the dimensions of the artificial objects, a test grid was built similar to the one used in a previous study [3]. It consists of differently sized transparent Triacontakaidigons (32-sided polygons) on a dark background, each specified by the diameter of the biggest circle fitting inside the Triacontakaidigon as shown in Fig. 14. The test grid optical images are 8-bit with size corresponding to 43×32 μm^2 area. The median intensity inside the Triacontakaidigon was $v' = 170$ and the median background value was $u' = 10$, giving a 50% threshold level of $\theta = 1/2(u' + v') = 90$. Specified and measured diameters of Triacontakaidigons are summarized in Tab. 1. The last Triacontakaidigon was too small to be measured. For circles with diameter > 1 μm, measured values differ from specified values in the order of 1%. Similar quantification results were reported in a previous study [3] for the same set of Triacontakaidigons.

Now, returning back to our ring artificial bubbles, to quantify their dimension, first the 2D

Table 1. Specified and measured diameters of Triacontakaidigons.

Triacontakaidigon	**Specified diameter (μm)**	**Measured diameter (μm)**
1	10.0± 0.1	10.02
2	5.0 ± 0.1	5.03
3	3.0 ± 0.1	2.97
4	2.0 ± 0.1	1.96
5	5.0 ± 0.1	5.07
6	3.0 ± 0.1	3.02
7	2.0 ± 0.1	1.96
8	1.6 ± 0.1	1.55
9	1.0 ± 0.1	0.93
10	0.8 ± 0.1	0.58
11	0.4 ± 0.1	-

images constructed were segmented using gray level window slicing using threshold value $T = 0.5$. This results in a binary, black and white image of the bubbles with a ring. Applying morphological image processing, white ring bubbles with black background are filled with white while black ring bubbles with white background are filled with black. The later images were complemented to get white region inside the bubble and black background. Finally the number of white region pixels and their area is computed to get the total area of the bubble.

Figure 15 presents comparison between true object and measured object sizes for both white as well as black ring bubbles. Results showed that a systematic error is observed for objects in focus with radius ≤ 1.65 μm. Moreover, for objects in focus with radius > 1.65 μm, measurements showed that there is discrepancy of 0.66% for white ring object and 0.64% for black ring objects, between the true object size and measured size. In addition, a comparison was made between true object size and measured object size for objects shifted by 25%, 50%, 75% and 90%. The comparison was done for objects of size $0.9\mu\text{m} \leq r \leq 5\mu\text{m}$, to avoid negative values when mean absolute percentage error is calculated. Table 2 presents true and measured dimensions in the case of the shifted bubbles. Results clearly showed that size measurement of objects with white rings is slightly higher than that of objects with black rings the reason being that convolving a white ring object is different from convolving a black ring object given a PSF. When a white ring object with black background is convolved with a PSF, the contribution of the white ring for the convolution result is higher than that of a black ring. Specifically the blurring effect of the PSF differs in both cases. As a result, the segmentation will result different values of size measures for the same shift of focus. The results also showed that for the same shift above and below the focus, size measurement could differ by up to 3.6%.

Optics EXPRESS

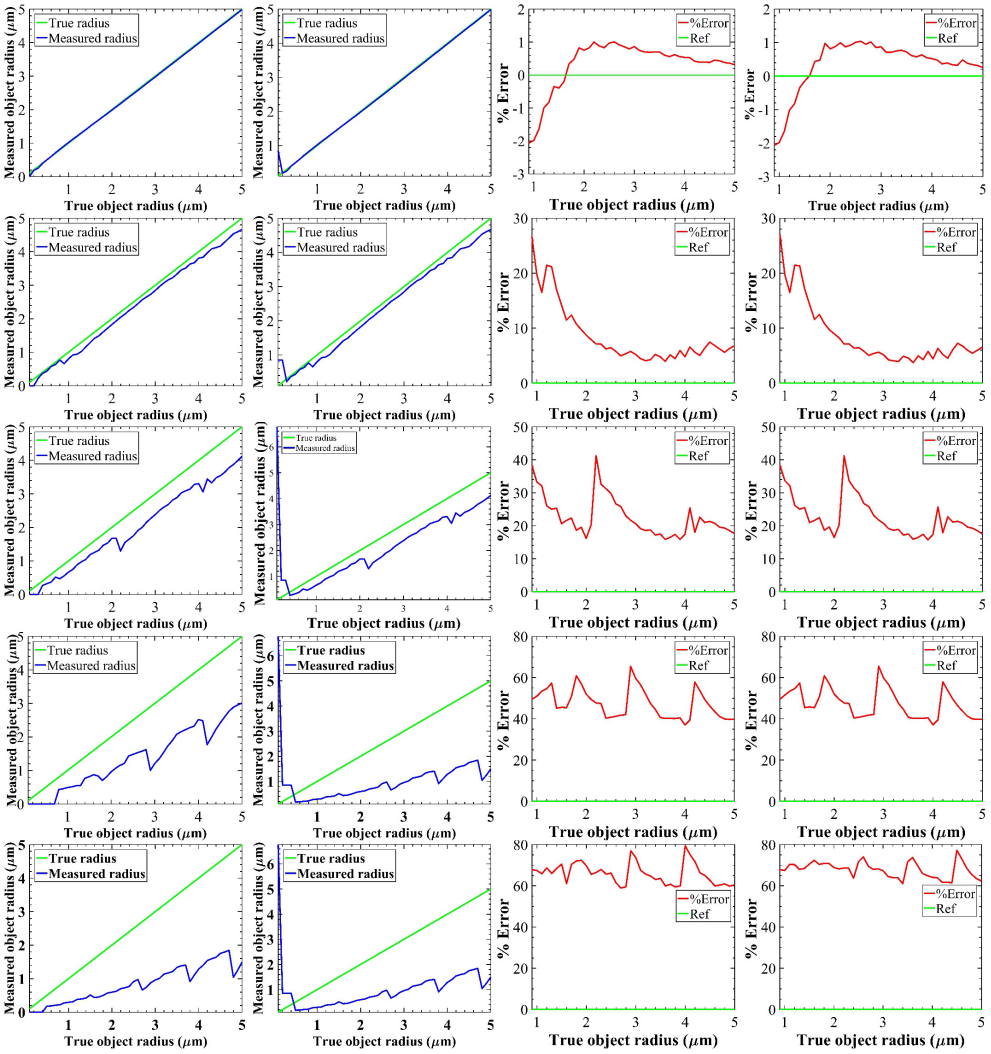

Fig. 15. Measured object diameter versus true object diameter at different shift values above focus: White ring object (first column) and Black ring object (second column); Object size measured percentage error at different shift values above focus: White ring objects (third column) and black ring objects (fourth column). Shift of focus is 25%, 50%, 75% and 90%, from top to bottom respectively.

Optics EXPRESS

Table 2 also explains the effect of defocusing in quantifying a microscope image of a microbubble. It is shown that effect of defocussing becomes more pronounced for shift of focus above 25%. In addition the mean percentage errors above and below focus are different. The reason is that the weighting function is not exactly symmetric; the weighting values below the focus are slightly greater than that of the weighting values above the focus.

Table 2. Comparison of black vs white ring object mean percentage errors for objects measured above and below focus.

Shift of focus (%)	**Mean percentage error for white ring object of (r >= 0.9 μm)**		**Mean percentage error for black ring object of (r >= 0.9 μm)**	
	Above focus	**Below focus**	**Above focus**	**Below focus**
25%	8.59380	5.96420	8.52160	5.86710
50%	22.6226	19.0577	22.7076	19.1277
75%	47.3440	42.5200	47.4123	42.5779
90%	67.9180	64.5743	67.9606	64.6048

5. Conclusion

This study introduced a novel technique to model a three-dimensional (3D) optical imaging system and quantification of the resulting simulated optical images. It is presented that even though a 3D object is in focus, its two-dimensional (2D) optical image size differs from the actual size. Artificial objects with different sizes were measured with an error less than 1% for an object with diameter greater than 1.65 μm, which is caused by the low resolution of the modeled object and the segmentation process. For smaller objects, the size measurement discrepancy between the actual and measured gets more pronounced. In addition, size measurements for smaller objects of actual radius < 0.9 μm of white rings with black background slightly differ from size measurements of black rings of same actual radius with white background. Furthermore, the effect of defocusing on object size measurement is also confirmed by the various tests carried out in this study. The study hopes to offer a standard for quantification of optical images of 3D objects and its future prospects to measure the actual size of an object from its defocused optical images.

Funding

The project "Smart Solutions in Ubiquitous Computing Environments", Grant Agency of Excellence, University of Hradec Kralove, Faculty of Informatics and Management, Czech Republic (ID: UHK-FIM-GE-2018); European Union's Horizon 2020 research and innovation programme under Marie Skłodowska-Curie grant agreement No 665790.

Disclosures

The authors declare that there are no conflicts of interest related to this article.